GEOPHYSICAL RESEARCH LETTERS, VOL. 37, L14306, doi:10.1029/2010GL043769, 2010



# Carbonate control of $H_2$ and $CH_4$ production in serpentinization systems at elevated P-Ts

L. Camille Jones,[1,2] Robert Rosenbauer,[2] Jonas I. Goldsmith,[1] and Christopher Oze[1]

Received 27 April 2010; revised 10 June 2010; accepted 21 June 2010; published 23 July 2010.

[1] Serpentinization of forsteritic olivine results in the inorganic synthesis of molecular hydrogen ($H_2$) in ultramafic hydrothermal systems (e.g., mid-ocean ridge and forearc environments). Inorganic carbon in those hydrothermal systems may react with $H_2$ to produce methane ($CH_4$) and other hydrocarbons or react with dissolved metal ions to form carbonate minerals. Here, we report serpentinization experiments at 200°C and 300 bar demonstrating $Fe^{2+}$ being incorporated into carbonates more rapidly than $Fe^{2+}$ oxidation (and concomitant $H_2$ formation) leading to diminished yields of $H_2$ and $H_2$-dependent $CH_4$. In addition, carbonate formation is temporally fast in carbonate oversaturated fluids. Our results demonstrate that carbonate chemistry ultimately modulates the abiotic synthesis of both $H_2$ and $CH_4$ in hydrothermal ultramafic systems and that ultramafic systems present great potential for $CO_2$-mineral sequestration. **Citation:** Jones, L. C., R. Rosenbauer, J. I. Goldsmith, and C. Oze (2010), Carbonate control of $H_2$ and $CH_4$ production in serpentinization systems at elevated P-Ts, *Geophys. Res. Lett.*, *37*, L14306, doi:10.1029/2010GL043769.

## 1. Introduction

[2] The near-surface inorganic production of diatomic hydrogen ($H_2$) via serpentinization (olivine hydrolysis) is a widespread and fundamental geochemical process resulting from the interaction of water and olivine-rich mantle material. Serpentinization of Mg-rich or forsteritic olivine produces $H_2$ via $Fe^{2+}$ oxidation and magnetite ($Fe_3O_4$) formation while also forming serpentine minerals ($Mg_3Si_2O_5(OH)_4$) and a variety of other minerals (i.e., brucite, talc, chlorite) [*Oze and Sharma*, 2007]. Laboratory experiments [e.g., *Berndt et al.*, 1996; *Hänchen et al.*, 2006; *Seyfried et al.*, 2007], field research [e.g., *Kelley et al.*, 2001; *Charlou et al.*, 2002; *Proskurowski et al.*, 2008] and thermodynamic studies [e.g., *Sleep et al.*, 2004; *Palandri and Reed*, 2004; *Oze and Sharma*, 2007] comprise a large and growing body of serpentinization research over a wide range of pressures-temperatures (P-Ts), mafic/ultramafic lithologies, water/rock ratios, and tectonic regimes. Elemental hydrogen evolved from serpentinization may react with aqueous and gaseous carbon ($CO_2$, $HCO_3^-$, HCOOH, etc.) in hydrothermal ultramafic systems such as mid-ocean ridges and forearc environments to produce methane ($CH_4$) and possibly a variety of hydrocarbons and organic compounds [e.g., *Horita and Berndt*, 1999; *McCollom and Seewald*, 2001; *Proskurowski et al.*, 2008]. This relationship between serpentinization and the abiogenic synthesis of organic compounds has received significant attention due to implications for: 1) the maintenance of life in present-day ultramafic-hosted hydrothermal systems, 2) the synthesis of precursor organic compounds related to the development of life, and 3) the formation of hydrocarbon energy resources.

[3] The behavior of aqueous carbonate species in serpentinization systems, such as at Lost City (Mid-Atlantic Ridge) or in carbon sequestration studies [e.g., *Goff and Lackner*, 1998; *Kelemen and Matter*, 2008], is important in its relationship to olivine hydrolysis and the resulting production of $H_2$ and $CH_4$. Not only do carbonates provide inorganic pathways for carbon speciation and sequestration, but the presence of carbonates may influence the kinetics and modulate the product distributions of serpentinization reactions. This study explores, under conditions similar to those present in mid-ocean ridge and forearc environments (200°C and 300 bar), the dynamic interplay between serpentinization of average Earth mantle olivine, the presence and formation of carbonates, and $H_2$ and $CH_4$ generation in carbonate over- and undersaturated systems.

## 2. Materials and Methods

[4] Olivine sand was prepared using multiple water rinses, sieving to 100 $\mu$m grain size, and sorting with a horizontal Franz magnetic separator. The average composition of olivine was $(Fe_{0.12}Mg_{0.88})_2SiO_4$ or $Fo_{88}$ based on ten analyses by electron microprobe microanalysis on an automated JEOL 733A electron microprobe (15 kV accelerating potential and a 15 nA beam current). The surface area for olivine was 0.9290 ± 0.0037 $m^2\ g^{-1}$ as determined using a multipoint $N_2$ BET isotherm analysis. The Fischer-Tropsch type (FTT) catalyst chromite ($(Fe_{0.24}Mg_{0.76})(Cr_{0.59}Al_{0.41})_2O_4$ from Yancy Co., N. Carolina) was included in all experiments to aid in carbon reduction [*Foustoukos and Seyfried*, 2004]. Chromite was powdered and processed similarly to olivine preparation. Olivine and chromite contained <0.04% total/organic carbon (LECO) providing a residual carbon source for $CH_4$ generation.

[5] Synthetic seawater was prepared with reagent grade KCl (0.0747 wt. %), $CaCl_2$ (0.205 wt. %), and NaCl (2.76 wt. %) in deionized water to approximate the typical 'evolved' seawater chemistry in mid-ocean ridge and forearc serpentinization sites [*Von Damm*, 1990]. Sulfur, a component in serpentinization systems, was excluded to simplify geochemical interactions. Sodium bicarbonate ($NaHCO_3$) was used as an additional carbon source. The seawater was purged with $N_2$ gas for ~ 24 h to minimize dissolved $CO_2$.

[6] Three hydrothermal experiments with varying amounts of carbonate were performed at 200°C and 300 bar using the parameters listed in Table 1. The olivine, chromite, and seawater provide multiple sources of carbon that in total are

[1]Bryn Mawr College, Bryn Mawr, Pennsylvania, USA.
[2]U.S. Geological Survey, Menlo Park, California, USA.


0094-8276/10/2010GL043769

**Table 1.** Reactants and Experimental Parameters

| Variable | Experiment 1[a] | Experiment 2[b] | Experiment 3[c] |
|---|---|---|---|
| Olivine ($Fo_{88}$) | 67.7 g | 67.7 g | 51.7 g |
| Chromite | 0.354 g | 0.354 g | 0.270 g |
| Evolved seawater[d] | 175 g | 174 g | 134 g |
| Sodium bicarbonate | - | 0.00914 g | 1.20 g |
| Water:Rock | 2.5: 1 | 2.5: 1 | 2.5: 1 |
| Pressure | 300 bar | 300 bar | 300 bar |
| Temperature | 200 °C | 200 °C | 200 °C |

[a]Carbonate undersaturated, no added C.
[b]Carbonate undersaturated, added C.
[c]Carbonate oversaturated, added C.
[d]See Materials and Methods.

well below carbonate saturation. Reactants were loaded into a flexible Au/Ti reaction cell and sealed in a rocking heated Cr-V alloy autoclave following the experimental approaches outlined by *Rosenbauer et al.* [1993]. Samples of the experimental fluid were periodically withdrawn via a Ti exit tube and a Ti sampling valve using gas-tight and sterile plastic syringes. The experiments were carried out in the Water-Rock Interaction Laboratory at the U.S. Geological Survey (Menlo Park, CA).

[7] Fluid samples were analyzed for total inorganic carbon (TIC) and pH immediately following sampling, and for Ca, Mg, and Fe concentrations. Carbon concentrations in the experimental fluids were measured as TIC with a CM 5012 $CO_2$ coulometer and with a CM 5130 acidification module. pH was measured with an Oakton series 500 pH meter and an Orion S103 Ross electrode. Elemental concentrations were measured on a Perkin-Elmer Sciex ELAN 6000 inductively coupled plasma mass spectrometer (ICP-MS).

[8] Elemental hydrogen and $CH_4$ were measured by gas chromatography (GC) using a Perkin-Elmer Sigma 3 gas chromatograph equipped with a thermal conductivity detector and an injection manifold capable of measuring the pressure of injection to within 0.1%.

[9] Residual solids were collected after depressurization and cooling and were sequentially extracted with dichloromethane, toluene, and dimethyl sulfoxide (DMSO). These extracts were analyzed for organic compounds by gas chromatography/mass spectroscopy (GC/MS); (Agilent 6890 gas chromatograph and Agilent 5973 mass selective detector). Solid samples were also ultrasonicated in DMSO for one minute to separate and refine potential organic residues from solid samples. The resulting deflocculated material was separated, dried, and analyzed using Fourier transform infrared (FT-IR) spectroscopy (Perkin Elmer Spectrum 2000 FT-IR). Final residual solids and isolated deflocculated material were evaluated using an FEI 600 Quanta FEG scanning electron microscope (SEM) with energy dispersive X-ray spectroscopy (EDS) capabilities. Surface areas for residual solids were determined using a multipoint $N_2$ BET isotherm analysis. The mineralogy of each sample was evaluated via X-ray diffraction (XRD) using a Rigaku Ultma IV base system with Bragg-Brentano/monochromator capabilities and operating at 40 kV and 40 mA.

## 3. Results

[10] Total inorganic carbon (TIC), dissolved gas, pH, and cation chemistry were monitored as a function of time throughout the experiments and rates were determined via linear regressions (Figure 1). In Exp. 1 (carbonate undersaturated, no added $NaHCO_3$), TIC was constant at 0.3 mmol $kg^{-1}$. In Exp. 2 (carbonate undersaturated, added $NaHCO_3$), initial TIC was 2.5 mmol $kg^{-1}$. Bicarbonate was reinjected into Exp. 2 at 626 h increasing TIC from near the detection limit to 0.46 mmol $kg^{-1}$. In Exp. 3 (carbonate oversaturated, added $NaHCO_3$), initial TIC was 89 mmol $kg^{-1}$ and decreased at a constant rate of 0.01 mmol $kg^{-1}$ $h^{-1}$ after an initial rapid decrease.

[11] Methane production was similar in Exps. 1 and 2, proceeding at rates of 0.10 and 0.06 $\mu$mol $kg^{-1}$ $h^{-1}$, respectively (Figure 1). However, in the carbonate oversaturated system (Exp. 3), $CH_4$ was produced at 0.01 $\mu$mol $kg^{-1}$ $h^{-1}$ during the first 1,000 h and then the rate increased 20-fold to 0.2 $\mu$mol $kg^{-1}$ $h^{-1}$ for the last 400 h. The pattern of $H_2$ evolution in these experiments was similar to that of $CH_4$ (Figure 1). Hydrogen production rates were 9.1 and 9.7 $\mu$mol $kg^{-1}$ $h^{-1}$ for Exps. 1 and 2, respectively. In the carbonate oversaturated system (Exp. 3), the rate of $H_2$ production was 2.5 $\mu$mol $kg^{-1}$ $h^{-1}$ for the first 1,000 h and then increased to a final rate of 10.2 $\mu$mol $kg^{-1}$ $h^{-1}$ for the last 400 h.

[12] pH values measured at 25°C (Figure 1) increased from 6 to 11 during the first 200 h for Exps. 1 and 2 and then remained constant. In the carbonate oversaturated system (Exp. 3), pH increased from 7 to 9.4 during the first 20 h and then remained constant. Calculated pHs at the experimental conditions (200°C and 300 bar) using SOLMINEQ are 7.7 (Exp. 1), 6.2 (Exp. 2), and 6.8 (Exp. 3) [*Kharaka et al.*, 1988].

[13] Concentrations of Ca (init. 11 mmol $kg^{-1}$), Mg (init. below detection limit), and Fe (init. 0.05 mmol $kg^{-1}$) in solution were monitored over time (Figure 1). In Exps. 1 and 2, Ca decreased at rates of 0.004 and 0.005 mmol $kg^{-1}$ $h^{-1}$, respectively. The small fluctuation of Ca in Exp. 2 corresponds with bicarbonate re-injection at 626 h. In Exp. 3, Ca decreased from 11 mmol $kg^{-1}$ to below 0.3 mmol $kg^{-1}$ (at a rate of 0.45 mmol $kg^{-1}$ $hr^{-1}$) within the first 24 h. In Exp. 1, Mg increased and then quickly decreased to near detection limits within 24 h. In Exp. 2, the Mg concentration prior to heating was 0.7 mmol $kg^{-1}$ and increased to 1.1 mmol $kg^{-1}$ during the first 24 h, and then decreased at a rate of 0.004 mmol $kg^{-1}$ $h^{-1}$ until achieving a steady value of 0.007 mmol $kg^{-1}$. Similarly, in Exp. 3, Mg in solution initially increased to 0.4 mmol $kg^{-1}$ and then rapidly decreased, in the first 24 h, to near the detection limit. Iron in solution fluctuated near its initial concentration during Exps. 1 and 2 and remained slightly lower (near 0.02 mmol $kg^{-1}$) in Exp. 3.

[14] End-member (defined as the final fluid, gas, or solid analyzed) experimental values are shown in Table 2 with their respective run times. Note that following depressurization and cooling of the hydrothermal experiments, dissolved Ca, Fe, and Mg concentrations increased, suggesting dissolution of mineral phases stable at 200°C and 300 bar.

[15] Mineral saturation indices (SIs) at 200°C and 300 bar were calculated using the aqueous concentration data and SOLMINEQ to determine if the experimental fluids were over- or undersaturated with respect to carbonate phases [*Kharaka et al.*, 1988]. Calculations of SIs show that all experiments progressed towards calcite ($CaCO_3$) equilibrium and that magnesite ($MgCO_3$) was always undersaturated. Most notably from these calculations, fluids in Exps. 1

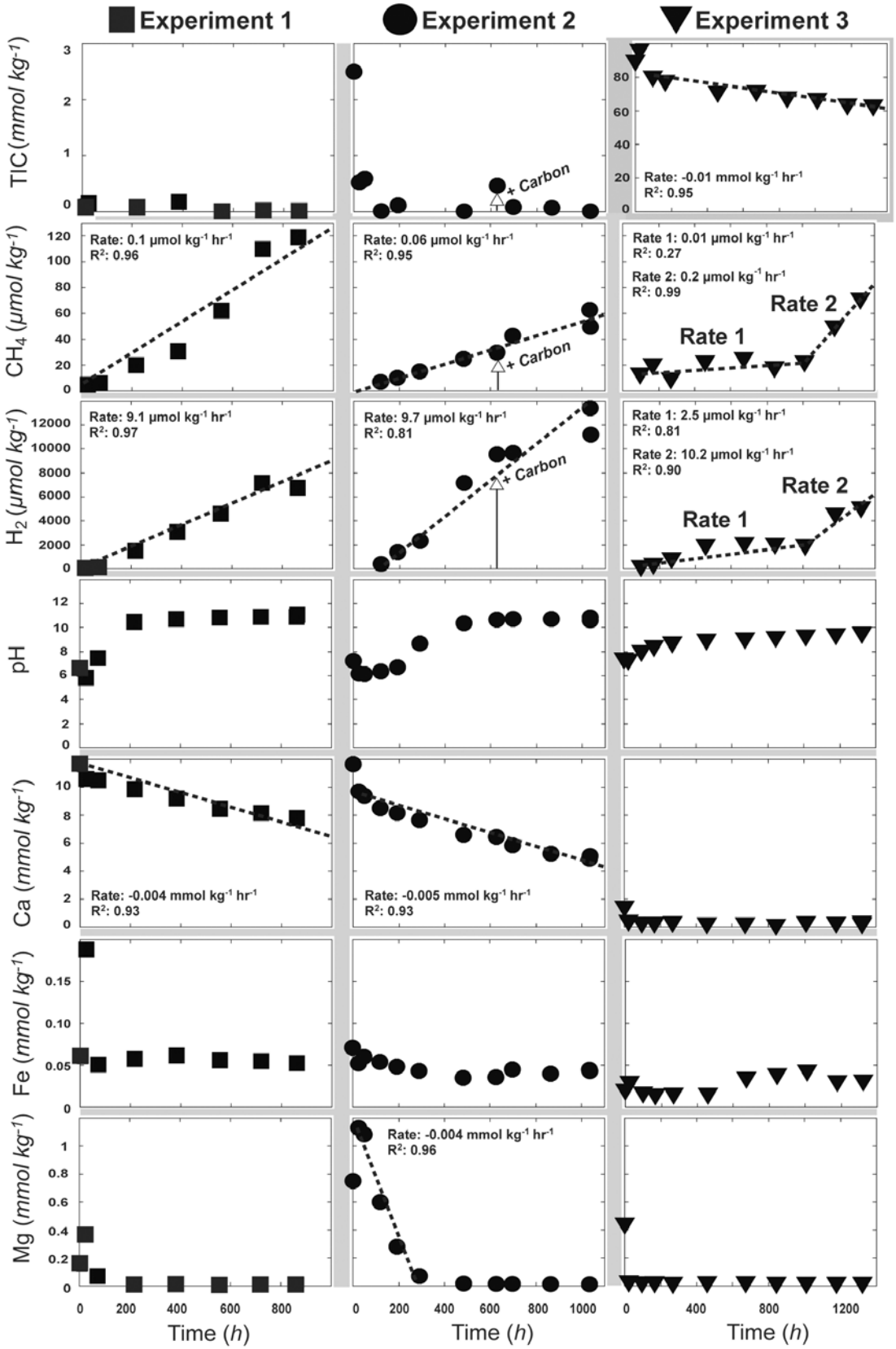


**Figure 1.** Total inorganic carbon (TIC; mmol $kg^{-1}$), $CH_4$ ($\mu$mol $kg^{-1}$), $H_2$ ($\mu$mol $kg^{-1}$), pH, and Ca, Fe, and Mg (mmol $kg^{-1}$) analyses collected over time (h) for Exps. 1–3 (Table 1). The time of bicarbonate reinjection in Exp. 2 is shown using a vertical arrow. Initial TICs were 0.09 mmol $kg^{-1}$ (Exp. 1), 2.5 mmol $kg^{-1}$ (Exp. 2), and 89 mmol $kg^{-1}$ (Exp. 3). End-member values are shown in Table 2. Each data point represents one analysis per withdrawn sample; calibration and controls constrain uncertainties with errors smaller than the symbol.

**Table 2.** Experimental Geochemical End-Member Results

| Variable | Experiment 1 | Experiment 2 | Experiment 3 |
|---|---|---|---|
| Host rock | Olivine ($Fo_{88}$) Chromite | Olivine ($Fo_{88}$) Chromite | Olivine ($Fo_{88}$) Chromite |
| Time (h) | 861 | 1,035 | 1,321 |
| T (°C) | 200 ± 1.1 | 200 ± 0.4 | 200 ± 2.8 |
| P (bar) | 300 ± 37 | 300 ± 13 | 300 ± 40 |
| pH (25 °C) | 10.92 | 10.70 | 9.40 |
| pH[a] (200°C) | 7.68 | 6.23 | 6.83 |
| TIC[b] (mmol/kg) | *b.d*[c] | *b.d.* | 62.0 |
| $CH_4$ (mmol/kg) | 0.119 | 0.056 | 0.070 |
| $H_2$ (mmol/kg) | 6.743 | 12.34 | 4.94 |
| Ca (mmol/kg) | 7.79 | 5.05 | 0.188 |
| Fe (mmol/kg) | 0.053 | 0.043 | 0.029 |
| Mg (mmol/kg) | 0.0042 | 0.079 | 0.0041 |
| Si (mmol/kg) | *b.d.* | *b.d.* | *b.d.* |
| Surface area ($m^2\ g^{-1}$) | 14.14 ± 0.03 | 23.61 ± 0.05[d] | 10.89 ± 0.02 |

[a]Calculated using SOLMINEQ.
[b]Total inorganic carbon.
[c]*b.d.*, below detection.
[d]Surface area at 1,367 h.

and 2 were siderite ($FeCO_3$) undersaturated while fluids in Exp. 3 were siderite oversaturated.

[16] Residual end-member solids from Exps. 1 and 2 are black in color and have a sticky texture despite being air-dried. Experiment 3 solids are unconsolidated, sandy, and light green in color. Surface area for end-member solids increased from the initial surface area of the starting material (0.9290 ± 0.0037 $m^2\ g^{-1}$) by more than ten-fold in all experiments (Table 2). Despite the black and sticky texture of the carbonate undersaturated solids (Exps. 1 and 2), organic extractions and GC/MS and FT-IR analyses did not yield evidence of any organic compounds. Dark DMSO-deflocculated material (not abundant in Exp. 3) was strongly magnetic suggesting that material was magnetite-rich (Figure 2a). White deflocculated material separated from all the experiment end-member solids was not magnetic. Based on these qualitative observations, magnetite was highly abundant in solids from the carbonate undersaturated experiments (Exps. 1 and 2) and was much scarcer in solids from the carbonate oversaturated system (Exp. 3).

[17] By SEM/EDS analysis, the short fibrous minerals in the white deflocculated material were determined to be chrysotile (Figure 2b) while the dark deflocculated material (Figure 2c) is an agglomeration of chrysotile, fine-grained magnetite, and potential organic solids. Experiment 2 solids contain olivine (large crystals), chrysotile, magnetite, a few ovoid-shaped nodules, and minor amounts of amorphous mineral surface coatings (Figure 2d). These ovoid nodules are more abundant in Exp. 3 (Figure 2e). Additionally, Exp. 3 solids contain less magnetite and fine-grained loose material as well as no noticeable amorphous surface coatings. Examination of these nodules with higher magnification (Figure 2f) in Exp. 3 solids revealed that they are dominantly composed of chrysotile/lizardite with interstitial carbonate and magnetite. The rounded grain morphology of these nodules is likely an artifact of the rocking autoclave. The presence of these ovoid nodules indicates the abundance of carbonate solids in the system. To summarize, chrysotile is present in all experiments, magnetite is more abundant in Exps. 1 and 2 solids, and carbonate is more abundant Exp. 3 solids. XRD analysis supports these SEM analyses and shows that solids for all three experiments contain olivine, chrysotile/lizardite, magnetite, and chromite while calcite and siderite were detected *only* in the carbonate oversaturated end-member solids (Exp. 3). Brucite, talc, or Ni-Fe alloys were not clearly discernable via XRD.

## 4. Discussion

[18] Differences between $H_2$ and $CH_4$ generation rates in the experiments (Figure 1) signify that the reaction pathways governing olivine hydrolysis, $Fe^{2+}$ oxidation/magnetite formation, and carbonate formation are changing over the course of the experiments. The composition of the end-member solids can be used to deconvolute these reaction pathways. The presence of chrysotile in all residual solids shows that olivine hydrolysis occurred in all experiments. The abundance of magnetite and steady production of $H_2$ and $CH_4$ in the carbonate undersaturated systems (Exps. 1 and 2) suggest that $Fe^{2+}$ oxidation and magnetite formation provided a continual and stable pathway for $H_2$ generation.

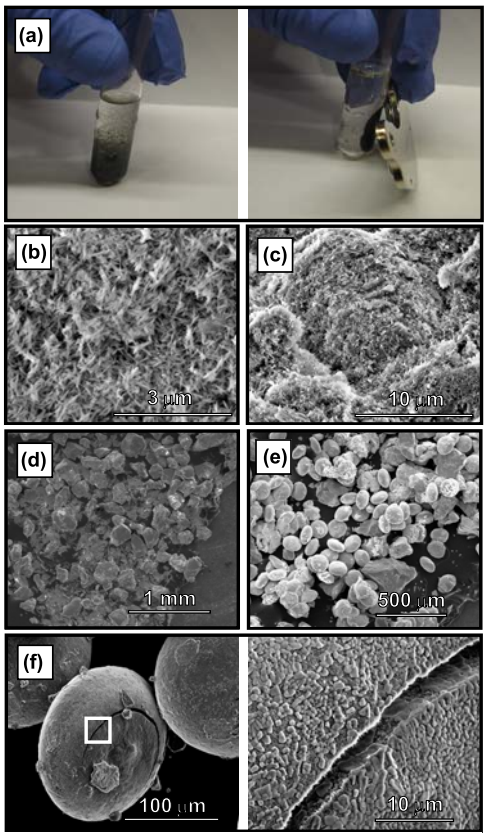


**Figure 2.** (a) Deflocculated material from Exp. 2 is shown (left) in suspension and (right) with a strong magnet. Scanning electron microprobe (SEM) images of (b) white deflocculated material from Exp. 2 where the short fibrous material is chrysotile (50,000 ×), (c) dark deflocculated material from Exp. 2 where both chrysotile and magnetite are abundantly present (15,000 ×), (d) end-member Exp. 2 solids with olivine (larger grains) and fine material (100 ×), (e) end-member Exp. 3 with olivine (larger grains) and abundant ovoid nodules (180 ×), and (f) magnification of ovoid nodule which is composed of chrysotile, carbonate, and magnetite. Magnifications are (left) 1,200 × and (right) 10,000 ×.

The presence of calcite/siderite and comparatively less magnetite in the carbonate oversaturated system (Exp. 3) and the slow rate of $H_2$ production during the first 1,000 h of the experiment provide evidence that carbonate formation occurs preferentially over $Fe^{2+}$ oxidation and magnetite formation. The increase in the rate of $H_2$ and $CH_4$ production in Exp. 3 after 1,000 h is likely due to $Fe^{2+}$ oxidation becoming competitive with calcite/siderite formation as the concentration of aqueous carbonate species decreased.

[19] Calculations show that fluid samples from Exps. 1 and 2 were always undersaturated with respect to siderite ($FeCO_3$); however, Exp. 3 fluids were siderite oversaturated and the thermodynamically favorable formation of siderite provides a non-oxidative route for $Fe^{2+}$ to react in this system. In total, these data suggest that, in the presence of excess aqueous carbonate species, $Fe^{2+}$ oxidation and $H_2$ formation is not kinetically competitive with siderite/calcite formation until much of the aqueous carbonate species are removed from solution via carbonate mineral precipitation (this occurred after 1,000 h in the carbonate oversaturated system). The trends in $CH_4$ production follow the same logic. Methane production proceeded similarly in Exps. 1 and 2 despite different levels of carbon suggesting that $H_2$ availability is a key factor in abiogenic $CH_4$ formation. This is supported by Exp. 3 where, despite high levels of carbon, $CH_4$ only began to form in appreciable quantities when $H_2$ production increased. The mineralogical and thermodynamic analyses corroborate this interpretation and show that the competition of $Fe^{2+}$ incorporation into carbonate solid phases versus oxidative magnetite formation plays an important role governing $H_2$ and $CH_4$ production. Overall, the presence of excess aqueous carbonate will result in less $H_2$ and $CH_4$ in serpentinization systems.

[20] Based on our results, the addition of large amounts of inorganic carbon into hydrothermal serpentinization systems (as in undersea industrial-scale carbon sequestration) will *not* enhance abiotic $CH_4$ production. This is important as $CH_4$ is more powerful as a greenhouse gas compared to $CO_2$. As we have shown, $CH_4$ production via serpentinization proceeds much more rapidly when hydrothermal solutions are carbonate undersaturated. In other olivine-rich environments, there will be a 'background' level of $CH_4$ being produced via serpentinization, even if minimal carbon is present. Our results indicate that the addition of excess inorganic carbon would both slow the natural production of $H_2$-$CH_4$ as well as lead to significant carbon sequestration via rapid calcite formation. When excess inorganic carbon is no longer supplied or the system reaches carbonate equilibrium, $CH_4$ production will return to comparable production rates limited by $Fe^{2+}$ oxidation.

[21] Rapid formation of carbonate minerals in the carbonate oversaturated system (Exp. 3) is indicated by the rapid drop in aqueous TIC and Ca in the first 24 h and the abundance of carbonates in end-member solids. This result provides insight into how methodologies for $CO_2$ sequestration in elevated P-T environments, not limited to serpentinization systems, may proceed. Calcite formation in carbonate oversaturated seawater with 11 mmol $kg^{-1}$ Ca is both thermodynamically favorable and rapid at 200°C and 300 bar. One $km^3$ of such seawater contains $4.4x10^8$ kg of Ca that could react in the presence of excess carbonate, at the rate of formation calculated above (0.45 mmol $kg^{-1}$ $hr^{-1}$), to form $1.1x10^9$ kg of calcite in 24 h, assuming favorable physical formation properties. The amount of carbon sequestered in $1.1x10^9$ kg of calcite is equivalent to that released from the combustion of $5x10^7$ gallons of gasoline. To put this in perspective, the United States consumes ~$3.8x10^8$ gallons of automobile gasoline per day (available from the U.S. Energy Information Administration at http://tonto.eia.doe.gov/ask/gasoline_faqs.asp). In a hydrothermal carbonate oversaturated circulation system, Ca present in ~7 $km^3$ of seawater would be required to react and sequester all of the United States' daily automobile $CO_2$ emissions as calcite. Carbon sequestration in other geologic environments, such as deep wells in basalt as shown in laboratory experiments by *McGrail et al.* [2006] and *Rosenbauer and Bischoff* [2009], demonstrate similar promise as long as ions including Ca, Mg, and $Fe^{2+}$ are supplied or are available at a rate comparable to carbon input.

## 5. Summary

[22] Experimental serpentinization results demonstrate that $H_2$ and $CH_4$ production proceeds more rapidly in carbonate undersaturated systems (9.1–9.7 $\mu$mol $H_2$ $kg^{-1}$ $h^{-1}$ and 0.06–0.10 $\mu$mol $CH_4$ $kg^{-1}$ $h^{-1}$) compared to the carbonate oversaturated systems (2.5 $\mu$mol $H_2$ $kg^{-1}$ $h^{-1}$ and ~$10^{-5}$ $\mu$mol $CH_4$ $kg^{-1}$ $h^{-1}$). After early and rapid carbonate formation in the carbonate oversaturated system, $H_2$ and $CH_4$ production rates increased to production rates comparable to the carbonate undersaturated systems due to the removal of excess aqueous carbonate species. These results help resolve issues related to laboratory and field $H_2$-$CH_4$ measurements and the sequestration of carbon in ultramafic and other geologic systems.

[23] **Acknowledgments.** We thank Bill Evans and John Fitzpatrick for analytical expertise and support and Norm Sleep, Renee Takesue, and Burt Thomas for critical reviews of this work. Any use of trade, product, or firm names in Isis Web pages, documents, or publications is for descriptive purposes only and does not imply endorsement by the U.S. government.

## References

Berndt, M. E., D. E. Allen, and W. E. Seyfried (1996), Reduction of $CO_2$ during serpentinization of olivine at 300°C and 500 bar, *Geology*, *24*, 351–354, doi:10.1130/0091-7613(1996)024<0351:ROCDSO>2.3.CO;2.

Charlou, J. L., et al. (2002), Geochemistry of high $H_2$ and $CH_4$ vent fluids issuing from ultramafic rocks at the Rainbow hydrothermal field (36°14′N, MAR), *Chem. Geol.*, *191*, 345–359, doi:10.1016/S0009-2541(02)00134-1.

Foustoukos, D. I., and W. E. Seyfried (2004), Hydrocarbons in hydrothermal vent fluids: The role of chromium-bearing catalysts, *Science*, *304*, 1002–1005, doi:10.1126/science.1096033.

Goff, F., and K. S. Lackner (1998), Carbon dioxide sequestering using ultramafic rocks, *Environ. Geosci.*, *5*, 89–102, doi:10.1046/j.1526-0984.1998.08014.x.

Hänchen, M., et al. (2006), Dissolution kinetics of fosteritic olivine at 90–150°C including effects of the presence of $CO_2$, *Geochim. Cosmochim. Acta*, *70*, 4403–4416, doi:10.1016/j.gca.2006.06.1560.

Horita, J., and M. E. Berndt (1999), Abiogenic methane formation and isotopic fractionation under hydrothermal conditions, *Science*, *285*, 1055–1057, doi:10.1126/science.285.5430.1055.

Kelemen, P. B., and J. Matter (2008), In situ carbonation of peridotite for $CO_2$ storage, *Proc. Natl. Acad. Sci. U. S. A.*, *105*, 17,295–17,300, doi:10.1073/pnas.0805794105.

Kelley, D. S., et al. (2001), An off-axis hydrothermal vent field near the Mid-Atlantic Ridge at 30°N, *Nature*, *412*, 145–149, doi:10.1038/35084000.

Kharaka, Y. K., et al. (1988), SOLMINEQ88, A computer program for geochemical modeling of water-rock interactions, *U.S. Geol. Surv. Water Resour. Invest. Rep., 88-4227*, pp 420.

McCollom, T. M., and J. S. Seewald (2001), A reassessment of the potential for reduction of dissolved $CO_2$ to hydrocarbons during serpentinization of olivine, *Geochim. Cosmochim. Acta*, *65*, 3769–3778, doi:10.1016/S0016-7037(01)00655-X.

McGrail, B. P., et al. (2006), Potential for carbon dioxide sequestration in flood basalts, *J. Geophys. Res.*, *111*, B12201, doi:10.1029/2005JB004169.

Oze, C., and M. Sharma (2007), Serpentinization and the inorganic synthesis of $H_2$ in planetary surfaces, *Icarus*, *186*, 557–561, doi:10.1016/j.icarus.2006.09.012.

Palandri, J. L., and M. H. Reed (2004), Geochemical models of metasomatism in ultramafic systems: Serpentinization, rodingitization, and sea floor carbonate chimney precipitation, *Geochim. Cosmochim. Acta*, *68*, 1115–1133, doi:10.1016/j.gca.2003.08.006.

Proskurowski, G., et al. (2008), Abiogenic hydrocarbon production at Lost City hydrothermal field, *Science*, *319*, 604–607, doi:10.1126/science.1151194.

Rosenbauer, R. J., and J. L. Bischoff (2009), $CO_2$ sequestration by basalt: Experimental studies and geochemical modeling, *Geochim. Cosmochim. Acta*, *73*, suppl., A1118.

Rosenbauer, R. J., J. L. Bischoff, and J. M. Potter (1993), A flexible Au-Ir cell with quick assembly for hydrothermal experiments, *Am. Mineral.*, *78*, 1286–1289.

Seyfried, W. E., D. I. Foustoukos, and Q. Fu (2007), Redox evolution and mass transfer during serpentinization: An experimental and theoretical study at 200°C, 500 bar with implications for ultramafic-hosted hydrothermal systems at mid-ocean ridges, *Geochim. Cosmochim. Acta*, *71*, 3872–3886, doi:10.1016/j.gca.2007.05.015.

Sleep, N. H., et al. (2004), $H_2$-rich fluids from serpentinization: Geochemical and biotic implications, *Proc. Natl. Acad. Sci. U. S. A.*, *101*, 12,818–12,823, doi:10.1073/pnas.0405289101.

Von Damm, K. L. (1990), Seafloor hydrothermal activity: black smoker chemistry and chimneys, *Annu. Rev. Earth Planet. Sci.*, *18*, 173–204, doi:10.1146/annurev.ea.18.050190.001133.

J. I. Goldsmith, L. C. Jones, and C. Oze, Bryn Mawr College, 101 N. Merion Ave., Bryn Mawr, PA 19010, USA. (christopher.oze@canterbury.ac.nz)

R. Rosenbauer, U.S. Geological Survey, 345 Middlefield Rd., Menlo Park, CA 94025, USA.